Desalination and Water Treatment
www.deswater.com

doi: 10.5004/dwt.2017.21355

92 (2017) 108–115
October

Hydrothermal synthesis of SnS_2 nanocrystals for photocatalytic degradation of 2,4,6-trichlorophenol under white LED light irradiation

Kezhen Qi[a], Sreejith Karthikeyan[b], Woolcheol Kim[c], Faisal Al Marzouqi[d], Ibrahim Said Al-Khusaibi[e], Younghun Kim[c,*], Rengaraj Selvaraj[d,*]

[a]*Institute of Catalysis for Energy and Environment, College of Chemistry and Chemical Engineering, Shenyang Normal University, Shenyang 110034, China*
[b]*Department of Physics and Nanotechnology, SRM Research Institute, SRM University, Kattankulathur, Chennai 603 203, Tamil Nadu, India*
[c]*Department of Chemical Engineering, Kwangwoon University, Seoul 139-701, Korea, Tel. +822 940 5768; email: korea1@kw.ac.kr (Y. Kim)*
[d]*Department of Chemistry, College of Science, Sultan Qaboos University, Muscat, Oman, Tel. +968 2414 2436; email: srengaraj1971@yahoo.com (R. Selvaraj)*
[e]*Central Analytical and Applied Research Unit, College of Science, Sultan Qaboos University, Muscat, Oman*

Received 22 June 2017; Accepted 24 August 2017

ABSTRACT

In this study, SnS_2 nanocrystals with controlled morphology were successfully synthesized by a simple hydrothermal method using thiosemicarbazide both as a sulfur source and as a capping agent. The X-ray powder diffraction analysis confirmed the hexagonal phase of these as-prepared SnS_2 nanocrystals. Morphological features were studied by field-emission scanning electron microscopy, indicating that the as-prepared SnS_2 crystals were nanoparticles. The optical property was studied by ultraviolet–visible diffused reflectance spectroscopy, indicating that the bandgap of SnS_2 samples is ~2.2 eV. Under white LED light irradiation (λ = 450 nm), the as-prepared SnS_2 nanocrystals exhibited a high photocatalytic activity for degrading 2,4,6-trichlorophenol solution. This work suggests that SnS_2 nanocrystal is a potential photocatalyst for detoxification.

Keywords: Hydrothermal synthesis; SnS_2 nanocrystals; LED light; Photocatalytic activity; 2,4,6-Trichlorophenol

1. Introduction

Chlorophenols (CPs), the most common organic pollutants widely used in agriculture and industry, are a serious environmental problem [1–3]. Most of the CPs are toxic, mutagenic, and carcinogenic, causing serious impact on our environment, even leading to the death of animals and plants [2,3]. Removal of these serious pollutants of CPs from the wastewater is very critical, because they will damage the vital organs of humans. The Agency for Toxic Substances and Disease Registry classified some of the chlorophenols (2-CP, 2,4-DCP, 2,4,6-TCP, and PCP) as the toxic substances according to the presented high toxic, carcinogenic, and bioaccumulation [4]. 2,4,6-Trichlorophenol (2,4,6-TCP) is one of the most severe pollutants among the CPs and is often used to test the efficiency of oxidation methods [5]. In order to prevent pollution, researchers used various methods to remove CPs from the wastewater, including chemical and biological methods [6,7]. Since Fujishima and Honda [8] observed the phenomenon of the photoelectrochemical splitting of water on semiconductor, photocatalysts have received extensive attention for removing the organic pollutants, including destruction of CPs in aqueous wastes [9–15].

Photocatalysis is based on the principle that when a semiconductor is exposed to a light source of appropriate

* Corresponding author.

wavelength, the positive holes in the valence band (VB) are appearing as the electrons are excited from the VB to the conduction band. If the generated electron–hole pair avoids recombination, they can move to the semiconductor surface and react with organic pollutants properly to degrade them into non-hazardous by-products. TiO_2-based photocatalysts have been most widely studied in the field of photocatalysis [16–21]. However, the big bandgap of TiO_2 (~3.2 eV) restricts its wide application. Besides TiO_2, ZnO has been intensively studied owing to its photosensitivity, non-toxic nature, abundant availability, and low cost [22,23]. Compared with TiO_2, ZnO absorbs a larger portion of the UV light [24,25]. However, one of the main problems with ZnO is still that it can be activated only by UV light, because of its big bandgap (~3.37 eV). In fact, the solar spectrum consists of 4% UV and 42% visible light. CdS is a suitable visible light sensitizer for ZnO, not only because of its narrow bandgap (~2.42 eV), but also because of the CdS crystal lattice match the ZnO crystal lattice well, easily forming the heterojunction between CdS and ZnO crystals [26]. This PN junction of ZnO/CdS can speed up the carrier transport at the interface [27]. Indeed, coupling with a narrow bandgap semiconductor such as CdS, $CuWO_4$, PbS and Ag_2S is an effective way to solve this problem [28–35].

N-type tin disulfide (SnS_2) with a bandgap of ~2.2 eV is a promising visible-light photocatalyst, consisting of a CdI_2-type crystal structure and the Sn cations are embedded between two layers of S anions [36]. Beside, SnS_2 also exhibits very good stability in acid solutions [37] and has also been used in solar cell and anode for lithium-ion battery owing to its excellent optoelectronic properties [38,39]. Besides the phase, the morphology, and size are also the key factors defining their photocatalytic performance, and these factors ultimately depend on the method of preparation. Various nanostructures of SnS_2 such as nanoflakes [37], nanosheets [36], and nanoflowers [40] have been successfully synthesized by various methods [41,42]. However, finding an easy route to synthesize SnS_2 nanocrystals with controlled morphology is still challenging.

In this study, a sample hydrothermal method is presented to prepare SnS_2 nanocrystals with controlled morphology. The major advantages of this synthesis method are the controllable SnS_2 morphologies, the attractive effect of preventing agglomeration during the nanoparticles formation, and the homogeneity of the nanoparticles prepared. Furthermore, the photocatalytic performance of the as-prepared nanocrystals was studied via the degradation of 2,4,6-TCP under white LED light irradiation. The as-synthesized SnS_2 nanocrystals showed a high photocatalytic activity in degrading 2,4,6-TCP solution, suggesting that SnS_2 nanocrystals will be a potential candidate for photocatalytic detoxification.

2. Experimental

2.1. Chemicals and preparation

Tin(IV) chloride (99%), thiosemicarbazide (99%), 2,4,6-TCP (99%), and methanol (99%) were purchased from Sigma-Aldrich (USA) and used as received without additional purification. All the solutions prepared throughout the experiment were used deionized and doubly distilled water. The synthesis of SnS_2 nanocrystals was performed as follows: 1.0 mmol of $SnCl_4$ and 3.0 mmol of thiosemicarbazide were put together in 80 mL of water and stirred vigorously for 30 min. The above solution was then transferred into an autoclave and maintained at 160°C for 6–24 h. Then, the autoclave was taken out and naturally cooled down to room temperature. The resulting precipitate was separated by centrifugation, and washed several times by distilled water and absolute ethanol. These products were finally dried in an oven at 70°C for 24 h and characterized by various spectroscopic techniques.

2.2. Characterization

The phase of these samples was investigated by PANalytical X PERT PRO (PW3040/60) X-ray diffractometer equipped with graphite monochromatized Cu K_α radiation (λ = 1.540 Å). The morphological features were examined by field-emission scanning electron microscopy (FESEM) using a JEOL JEM-3010 microscope, installed with an energy-dispersive spectroscopy (EDS). X-ray photoelectron spectroscopy (XPS) was conducted using a Sigma Probe (Thermo VG, UK) X-ray photoelectron spectrometer, with Al K_α radiation (1.486 eV) source and a pass energy of 20 eV. The absorption spectra of the as-prepared samples were recorded using a spectrophotometer (V-670, JASCO) in the wavelength range of 200 and 1,000 nm, with $BaSO_4$ as a reference.

2.3. Photocatalytic degradation of 2,4,6-trichlorophenol

The details of photocatalytic activity test can be found from Rengaraj et al. [43,44], and only a few critical points are discussed here. A low powered LED provides visible light (λ = 450 nm) and the reaction is at 20°C. A special glass frit as an air diffuser uniformly disperses air into the solution. The photocatalytic activity study under visible light was performed with freshly prepared aqueous suspension: by adding 0.10 g of catalyst into 250 mL of magnetically stirred aqueous TCP solution (5 mg L^{-1}). The analytical samples were taken at the given time intervals, centrifuged, and filtered to remove the catalyst, then analyzed by liquid chromatography–mass spectrometry (LC/MS) (Model: Agilent Technologies 6460 Triple Quad LC/MS). The peak intensity was used to derive the degree of degradation of TCP, and the TCP concentration was also analyzed via the quad LC/MS.

3. Results and discussion

3.1. X-ray powder diffraction

X-ray powder diffraction (XRD) of SnS_2 samples derived from the hydrothermal reaction between $SnCl_4$ and thiosemicarbazide was recorded, as shown in Fig. 1. The data perfectly matched with that of hexagonal SnS_2 phase (JCPDS No. 40-146). No other peaks from impurities or secondary phase were present. The intensity of peaks increased with increasing reaction time. Lattice parameters were calculated for each sample and listed in Table 1 and found to be very close to the reported value (a = 3.647 Å and c = 5.898 Å). During the synthesis process, thiosemicarbazide hydrolyzes to release H_2S, followed by its dissociation to generate S^{2-}, then combining with Sn^{4+} to form SnS_2 [45]. Because S^{2-} release is a gradual

process, the nucleation rate of SnS_2 may be easily controlled by varying the reaction temperature and time. The intensity of XRD peaks increases with increasing reaction time. The full width half maxima of the samples decreased with increasing time via Lorentzian fitting. The crystalline sizes of SnS_2 nanoparticals were determined by the Debye–Scherrer equation [46,47].

3.2. Bandgap

The bandgap value was determined by Kubelka–Munk (K–M or $F(R)$) method. In this method, $F(R)$ is proportional to the absorption coefficient α according to the following relationship [48,49]:

$$F(R) = \frac{(1-R)^2}{2R}$$

where R is the reflectance. The dependence of the absorption coefficient (α) on the photon energy equation is given as follows.

$$\alpha h\upsilon = A(h\upsilon - E_g)^m$$

where h is Plank's constant, υ is the frequency, E_g is the bandgap energy, and A is the constant having separate values for different transitions. The values of m for allowed direct, allowed indirect, forbidden direct, and forbidden indirect transition are 1/2, 2, 3/2, and 3, respectively. The bandgap was calculated from the x-intercept from the straight portion of $(\alpha h\upsilon)^{1/m}$ vs. $h\upsilon$ plots. Since α is proportional to $F(R)$, $(F(R) \times h\upsilon)^2$ vs. $h\upsilon$ ($m = 1/2$) was plotted for finding the direct bandgap and for indirect bandgap used $(F(R) \times h\upsilon)^{1/2}$ vs. $h\upsilon$ for ($m = 2$) to find the indirect bandgap [50]. The absorbance vs. wavelength for all the samples is shown in Fig. 2, indicating a red shift in the band edge.

In this study, we used the modified Kubelka–Munk relation and plotted $(F(R) \times h\upsilon)^2$ vs. $h\upsilon$ to find the direct bandgap from the absorbance data. It is clear that the as-prepared SnS_2 samples fit well with the direct bandgap relation. The bandgap of these materials slightly decreased as the reaction duration increased from 6 to 24 h, while they are all very close to the reported value of 2.24 eV [51] (Fig. 3). The bandgap of the as-prepared SnS_2 samples decreased to 2.28, 2.26, and 2.23 eV for the synthesis time 6, 12, and 24 h, respectively, may be due to the morphology effect.

3.3. XPS analysis

Surface composition of the SnS_2 nanocrystals (24 h sample) was examined by XPS (Fig. 4). The XPS survey spectrum for different atoms, as shown in Fig. 4(A),

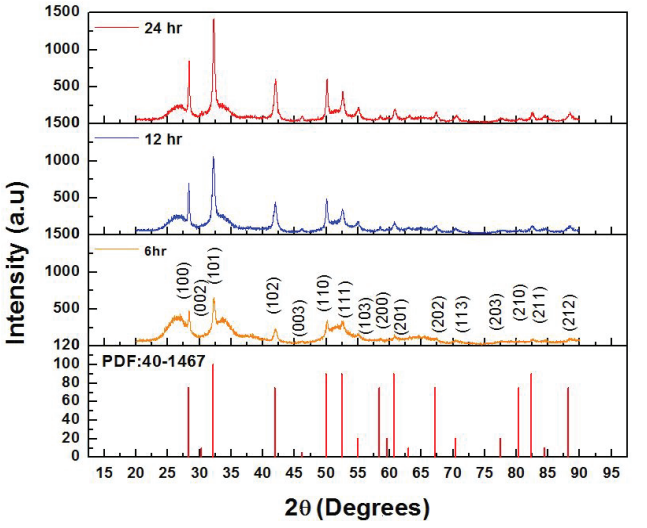

Fig. 1. XRD spectrum of SnS_2 crystals prepared at different reaction times.

Table 1
Lattice parameter and crystal size of SnS_2 particles prepared by the hydrothermal method at various reaction times

Sample	a (Å)	c (Å)	Crystal size (nm)
SnS_2 – 6 h	3.622	5.913	20.05
SnS_2 – 12 h	3.633	5.900	22.59
SnS_2 – 24 h	3.627	5.900	25.97

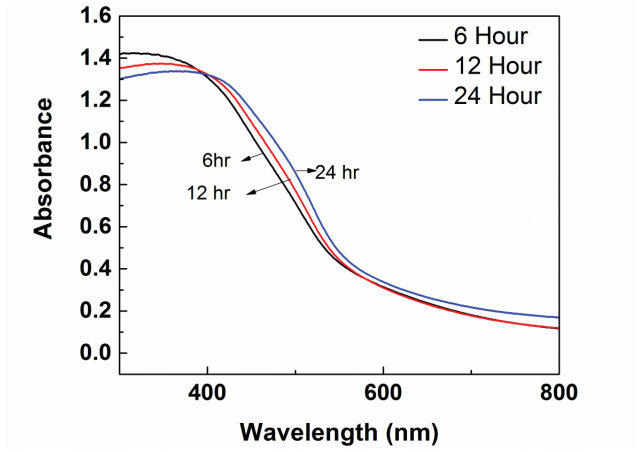

Fig. 2. Absorbance vs. wavelength for SnS_2 nanocrystals prepared at different reaction times (6, 12, and 24 h).

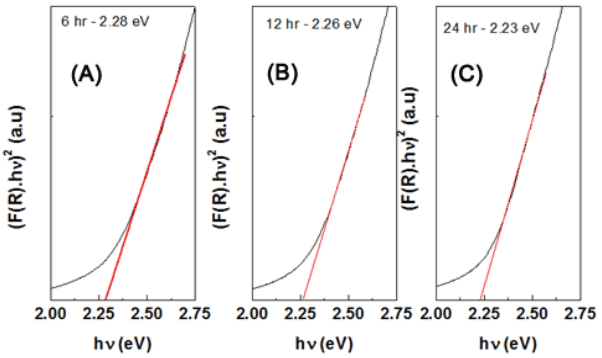

Fig. 3. Bandgap of SnS_2 samples prepared at different reaction times.

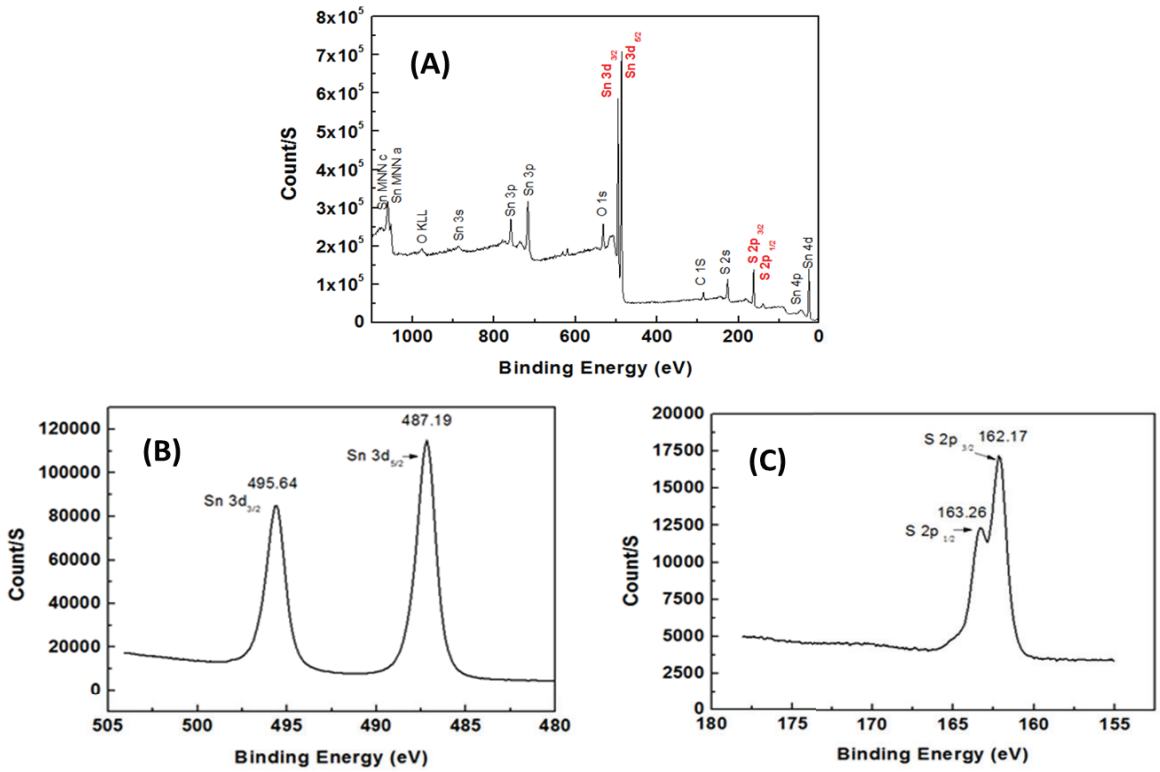

Fig. 4. XPS of SnS_2 nanocrystals synthesized with 24 h: (A) survey spectrum, (B) Sn 3d binding energy spectrum, and (C) S 2p binding energy spectrum.

indicates the presence of Sn, S, and a trace amount of C (C is from XPS instrument itself). Fig. 4(B) shows the two strong peaks at 487.19 and 495.64 eV, attributed to Sn $3d_{5/2}$ and $3d_{3/2}$, respectively, which are the characteristic of Sn^{4+} in SnS_2 [52]. No evidence of Sn^{2+} (binding energy at 485.8 eV) was detected in the spectra. Fig. 4(C) shows the peak at 162.17 and 163.26 eV and can be assigned to S $2p_{3/2}$ and S $2p_{1/2}$, respectively [52–54]. The integral peak area of Sn 3d and S 2p, the atomic ratio of Sn/S is 1:1.92, close to the stoichiometric ratio of SnS_2.

3.4. Morphology

Morphological features were studied by using FESEM as shown in Fig. 5. The sample prepared in 6 h exhibited a large cluster with a very soft edge. Grain size increased with increasing reaction time. The grain size of samples prepared for 12 and 24 h has been analyzed by using ImageJ. The measurement of 20 grains from different locations of the high-resolution SEM image indicated that the average grain size of 12 and 24 h samples was 112 and 127 nm, respectively. The sample prepared for 24 h exhibited a flake-like structure with an average thickness of 40 nm.

3.5. EDS analysis

The elemental composition of SnS_2 nanoparticles was studied by EDS. Fig. 6 shows the spectra of EDS data of 24 h sample. No other elements were detected in the EDS spectrum, confirming the elemental purity of the sample and atomic percentage was found close to 65% of Sn and 35% of S. Elemental mapping was performed to identify the uniformity of the elemental distribution (Fig. 7), using Sn Lα (green color) and S Kα (red color). The elemental mapping revealed the uniform distribution of elements throughout the sample. The EDS result as shown in Fig. 6 also reveals the coexistence of Sn and S. This result is in perfect agreement with the above XPS results (Fig. 4).

3.6. Photocatalytic activity

In SnS_2 nanocrystals, a fully ionized tin vacancy would generate four holes (h^+), whereas a sulfur vacancy would generate two e^-s. Therefore, SnS_2 with Sn vacancy is n-type and degrades the organic pollutant via reduction [55,56]. The photodegradation of pollutants by using SnS_2 is illustrated in Fig. 8. The photodegradation of 2,4,6-TCP using SnS_2 was inspected under white LED irradiation to evaluate their photoactivities. As reported previously, no direct photocatalysis of 2,4,6-TCP was found in the absence of catalysts as expected [57]. In order to assess the photocatalytic activity of SnS_2, experiments were performed as described in the experimental section. The photocatalytic activity of SnS_2 (24 h) is shown in Fig. 9, with an initial concentration of 5 mg L^{-1} under LED light irradiation in aqueous suspension. The time-dependent quad LC/MS peak intensities of the TCP solution are presented in Fig. 10, with SnS_2 as the photocatalyst. The peak appears at 0.9 min. After 120 min, no peak could be detected,

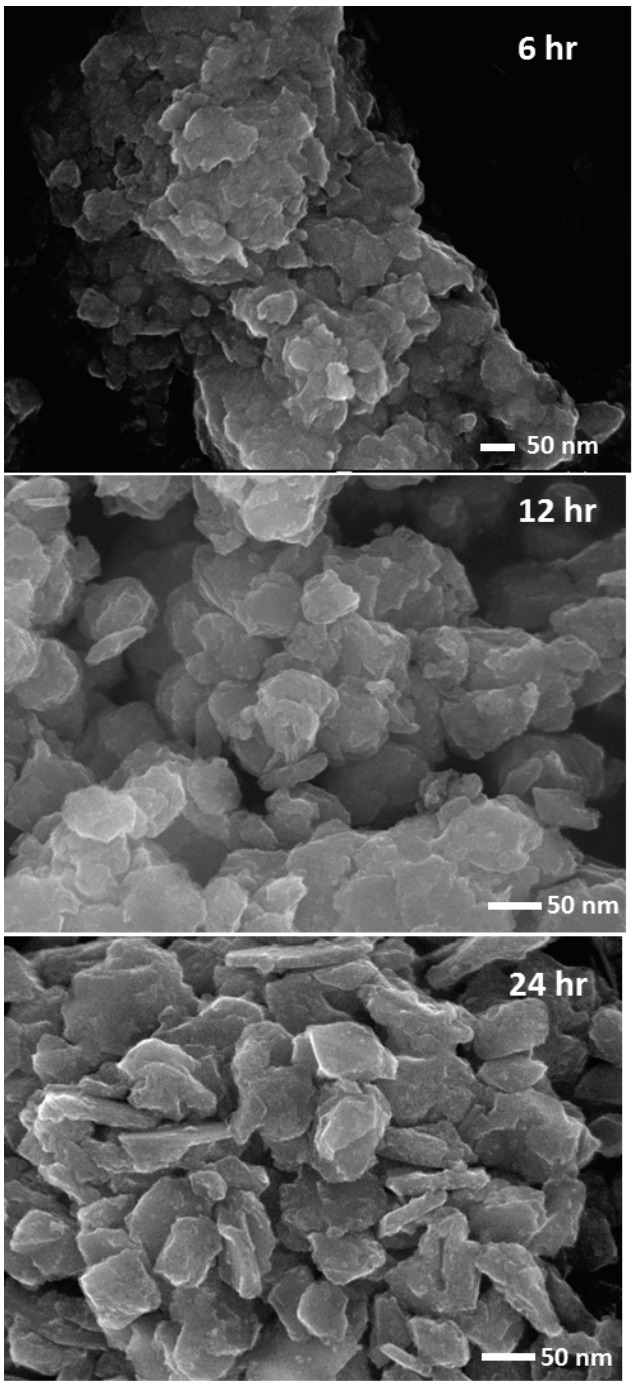

Fig. 5. SEM images of SnS_2 samples prepared for different reaction times.

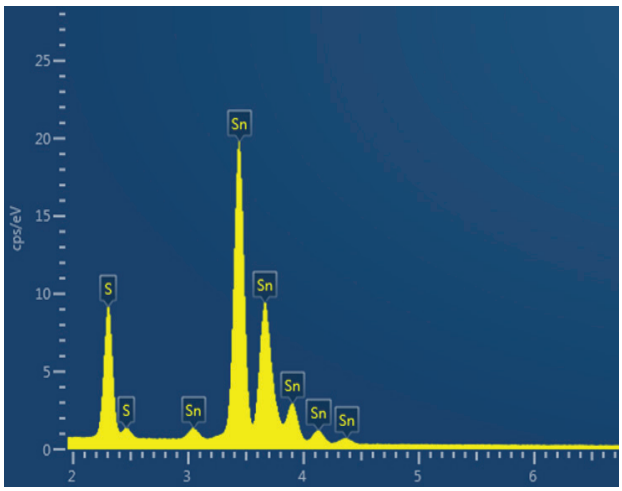

Fig. 6. EDS of SnS_2 nanocrystals prepared with 24 h.

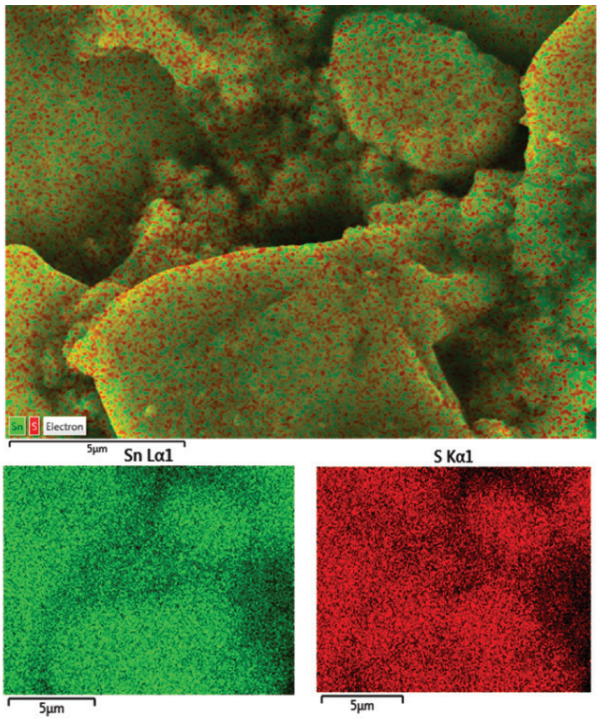

Fig. 7. Elemental mapping of Sn and S (24 h sample).

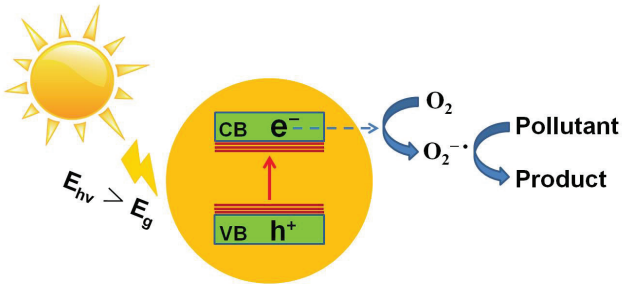

Fig. 8. Basic mechanism of SnS_2 photocatalysis.

so that the oxidation of TCP has already reached more than 95% completion in the presence of SnS_2 nanocrystals under white LED light irradiation.

The quad LC/MS degradation profile of TCP presented in Figs. 9 and 10 shows the rapid removal of TCP. TCP contains three chloro groups attached at 2-, 4-, and 6-position on the aromatic ring with respect to the position of –OH group. The presence of chloro groups generates additional centers for superoxide anion radicals ($O_2^{-\bullet}$) to

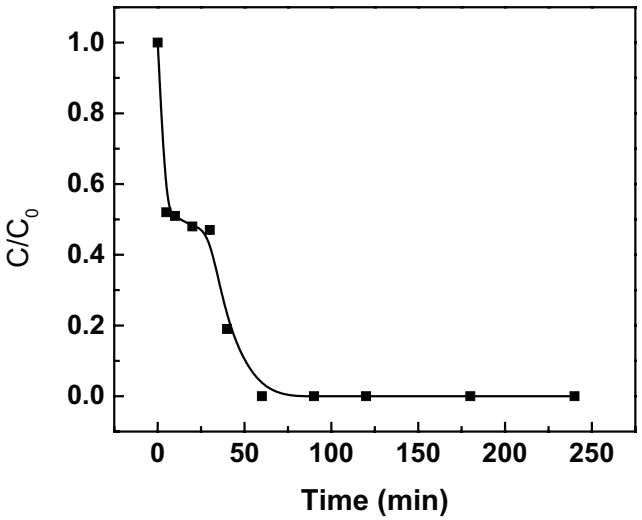

Fig. 9. Photocatalytic degradation of 2,4,6-TCP under white LED irradiation by SnS_2 nanocrystals (24 h sample).

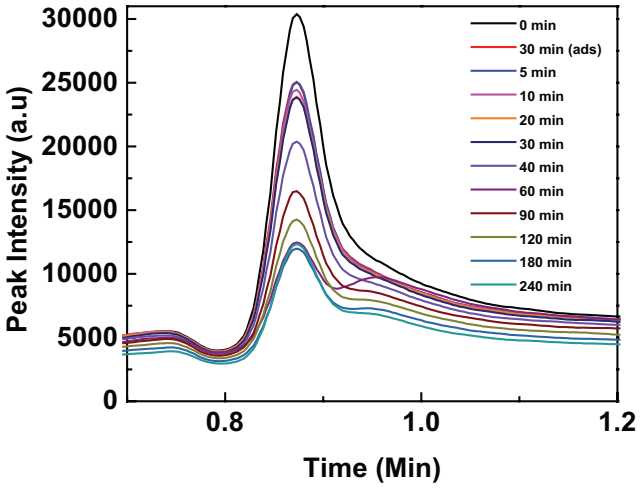

Fig. 10. Variation in 2,4,6-TCP degradation with time by SnS_2 nanocrystals (24 h sample) under white LED light irradiation.

attack, accelerating the degradation of TCP. And the formation of $O_2^{-\bullet}$ is contributed by the SnS_2 as schemed in Fig. 8. Therefore, 2,4,6-TCP degradation is indeed catalyzed by SnS_2. Besides, an interesting phenomenon can be observed that the degradation of 2,4,6-TCP appears suspiciously slow down shortly after the initiation of the degradation and lasts about 30 min and then gets faster again until the end for about 30 min. An explanation may be as follows: it is possible that the surface of ZnS_2 catalysts is surrounded by large amount of 2,4,6-TCP molecules via adsorption during the period of dark reaction, in which about half of the TCP has been degraded. Thus, the light absorption of SnS_2 can be retarded, which will slow down the rate of photocatalytic reaction. Once the catalytic reaction proceeds, the surface cover layer of the adsorbed 2,4,6-TCP molecules are broken down and the surface of the catalyst is better exposed to the light. Therefore, the rate of catalytic reaction accelerates at this stage.

4. Conclusion

In this study, morphology-controlled SnS_2 nanocrystals were successfully synthesized in a water system by using thiosemicarbazide, acting both as the capping agent and sulfur source. The XRD analysis revealed that the as-prepared nanocrystals are the hexagonal phase of SnS_2. The optical properties of the as-prepared SnS_2 nanocrystals exhibited a narrow bandgap of ~2.2 eV. More importantly, these synthesized SnS_2 nanocrystals showed a high photocatalytic activity in degrading of 2,4,6-TCP solution under white LED light irradiation. This study shows that SnS_2 nanocrystals will find potential application in visible-light photocatalytic detoxification.

Acknowledgments

This study was supported by SQU-Internal Grant research project (IG/SCI/CHEM/17/05) and the National Natural Science Foundation of China (51602207). The author Y. Kim would like to thank the National Research Foundation of Korea (NRF-2017R1A2B4001829).

Conflict of interest

The authors declare no competing financial interest.

References

[1] P. Vijayan, C. Mahendiran, C. Suresh, K. Shanthi, Photocatalytic activity of iron doped nanocrystalline titania for the oxidative degradation of 2,4,6-trichlorophenol, Catal. Today, 141 (2009) 220–224.
[2] S. Rengaraj, X.Z. Li, Enhanced photocatalytic activity of TiO_2 by doping with Ag for degradation of 2,4,6-trichlorophenol in aqueous suspension, J. Mol. Catal. A: Chem., 243 (2006) 60–67.
[3] S. Mozia, K. Bubacz, M. Janus, A.W. Morawski, Decomposition of 3-chlorophenol on nitrogen modified TiO_2 photocatalysts, J. Hazard. Mater., 203 (2012) 128–136.
[4] M. Nichkova, R. Galve, M.-P. Marco, Biological monitoring of 2,4,5-trichlorophenol (I): preparation of antibodies and development of an immunoassay using theoretical models, Chem. Res. Toxicol., 15 (2002) 1360–1370.
[5] G. Lente, J.H. Espenson, Oxidation of 2,4,6-trichlorophenol by hydrogen peroxide. Comparison of different iron-based catalysts, Green Chem., 7 (2005) 28–34.
[6] M. Pera-Titus, V. García-Molina, M.A. Baños, J. Giménez, S. Esplugas, Degradation of chlorophenols by means of advanced oxidation processes: a general review, Appl. Catal. B, 47 (2004) 219–256.
[7] G. Díaz-Díaz, M. Celis-García, M.C. Blanco-López, M.J. Lobo-Castañón, A.J. Miranda-Ordieres, P. Tuñón-Blanco, Heterogeneous catalytic 2,4,6-trichlorophenol degradation at hemin–acrylic copolymer, Appl. Catal. B, 96 (2010) 51–56.
[8] A. Fujishima, K. Honda, Electrochemical photolysis of water at a semiconductor electrode, Nature, 238 (1972) 37–38.
[9] S. Ahmed, M.G. Rasul, R. Brown, M.A. Hashib, Influence of parameters on the heterogeneous photocatalytic degradation of pesticides and phenolic contaminants in wastewater: a short review, J. Environ. Manage., 92 (2011) 311–330.
[10] V. Vo, T.P.T. Thi, H.Y. Kim, S.J. Kim, Facile post-synthesis and photocatalytic activity of N-doped ZnO–SBA-15, J. Phys. Chem. Solids, 75 (2014) 403–409.
[11] R. Saravanan, M.M. Khan, V.K. Gupta, E. Mosquera, F. Gracia, V. Narayanan, A. Stephen, ZnO/Ag/Mn_2O_3 nanocomposite for visible light-induced industrial textile effluent degradation, uric acid and ascorbic acid sensing and antimicrobial activity, RSC Adv., 5 (2015) 34645–34651.

[12] M.M. Khan, S.A. Ansari, M.E. Khan, M.O. Ansari, B.K. Min, M.H. Cho, Visible light-induced enhanced photoelectrochemical and photocatalytic studies of gold decorated SnO_2 nanostructures, New J. Chem., 39 (2015) 2758–2766.
[13] S. Cao, J. Yu, Carbon-based H_2-production photocatalytic materials, J. Photochem. Photobiol. C, 27 (2016) 72–99.
[14] Z. He, J. Fu, B. Cheng, J. Yu, S. Cao, $Cu_2(OH)_2CO_3$ clusters: novel noble-metal-free cocatalysts for efficient photocatalytic hydrogen production from water splitting, Appl. Catal. B, 205 (2017) 104–111.
[15] A. Etogo, R. Liu, J. Ren, L. Qi, C. Zheng, J. Ning, Y. Zhong, Y. Hu, Facile one-pot solvothermal preparation of Mo-doped Bi_2WO_6 biscuit-like microstructures for visible-light-driven photocatalytic water oxidation, J. Mater. Chem. A, 4 (2016) 13242–13250.
[16] S.K. Yadav, S.R. Madeshwaran, J.W. Cho, Synthesis of a hybrid assembly composed of titanium dioxide nanoparticles and thin multi-walled carbon nanotubes using "click chemistry", J. Colloid Interface Sci., 358 (2011) 471–476.
[17] Y. Park, W. Kim, H. Park, T. Tachikawa, T. Majima, W. Choi, Carbon-doped TiO_2 photocatalyst synthesized without using an external carbon precursor and the visible light activity, Appl. Catal. B, 91 (2009) 355–361.
[18] X. Hu, H. Ji, L. Wu, Singlet oxygen photogeneration and 2,4,6-TCP photodegradation at Pt/TiO_2 under visible light illumination, RSC Adv., 2 (2012) 12378–12383.
[19] T.K. Ghorai, Photocatalytic degradation of 4-chlorophenol by $CuMoO_4$-doped TiO_2 nanoparticles synthesized by chemical route, Open J. Phys. Chem., 1 (2011) 28–36.
[20] J. Low, B. Cheng, J. Yu, Surface modification and enhanced photocatalytic CO_2 reduction performance of TiO_2: a review, Appl. Surf. Sci., 392 (2017) 658–686.
[21] A. Meng, J. Zhang, D. Xu, B. Cheng, J. Yu, Enhanced photocatalytic H_2-production activity of anatase TiO_2 nanosheet by selectively depositing dual-cocatalysts on {101} and {001} facets, Appl. Catal. B, 198 (2016) 286–294.
[22] H. Ouyang, J.F. Huang, C. Li, L. Cao, J. Fei, Synthesis of carbon doped ZnO with a porous structure and its solar-light photocatalytic properties, Mater. Lett., 111 (2013) 217–220.
[23] S.J. Peatson, D.P. Norton, K. Ip, Y.W. Heo, T. Steiner, Recent progress in processing and properties of ZnO, Prog. Mater Sci., 50 (2005) 293–340.
[24] C.A.K. Gouvea, F. Wypych, S.G. Moraes, N. Duran, N. Nagata, P. Peralta-Zamora, Semiconductor-assisted photocatalytic degradation of reactive dyes in aqueous solution, Chemosphere, 40 (2000) 433–440.
[25] B. Dindar, S. Icli, Unusual photoreactivity of zinc oxide irradiated by concentrated sunlight, J. Photochem. Photobiol. A, 140 (2001) 263–268.
[26] S.L. Xiong, B.J. Xi, Y.T. Qian, CdS hierarchical nanostructures with tunable morphologies: preparation and photocatalytic properties, J. Phys. Chem. C, 114 (2010) 14029–14035.
[27] L. Stolt, J. Hedstrom, J. Kessler, M. Ruckh, K.O. Velthaus, H.W. Schock, ZnO/CdS/$CuInSe_2$ thin-film solar cells with improved performance, Appl. Phys. Lett., 62 (1993) 597.
[28] K. Ullah, Z.-D. Meng, S. Ye, L. Zhu, W.-C. Oh, Microalgal biofuels: flexible bioenergies for sustainable development, J. Ind. Chem. Eng., 20 (2014) 1035–1046.
[29] E.S. Aazam, Photocatalytic oxidation of methylene blue dye under visible light by Ni doped Ag_2S nanoparticles, J. Ind. Chem. Eng., 20 (2014) 4033–4038.
[30] K. Vignesh, R. Priyanka, R. Hariharan, M. Rajarajan, A. Suganthi, Fabrication of CdS and $CuWO_4$ modified TiO_2 nanoparticles and its photocatalytic activity under visible light irradiation, J. Ind. Chem. Eng., 20 (2014) 435–443.
[31] B. Zhu, P. Xia, Y. Li, W. Ho, J. Yu, Fabrication and photocatalytic activity enhanced mechanism of direct Z-scheme g-C_3N_4/Ag_2WO_4 photocatalyst, Appl. Surf. Sci., 391 (2017) 175–183.
[32] X. Li, J. Yu, M. Jaroniec, Hierarchical photocatalysts, Chem. Soc. Rev., 45 (2016) 2603–2636.
[33] Y. Hu, X. Gao, L. Yu, Y. Wang, J. Ning, S. Xu, X.W. (David) Lou, Carbon-coated CdS petalous nanostructures with enhanced photostability and photocatalytic activity, Angew. Chem., 21 (2013) 5746–5749.
[34] W. Yang, Y. Liu, Y. Hu, M. Zhou, H. Qian, Microwave-assisted synthesis of porous CdO–CdS core–shell nanoboxes with enhanced visible-light-driven photocatalytic reduction of Cr(VI), J. Mater. Chem., 22 (2012) 13895–13898.
[35] Y. Liu, L. Zhou, Y. Hu, C. Guo, H. Qian, F. Zhang, X.W. (David) Lou, Magnetic-field induced formation of 1D Fe_3O_4/C/CdS coaxial nanochains as highly efficient and reusable photocatalysts for water treatment, J. Mater. Chem., 21 (2011) 18359–18364.
[36] P. Chen, Y. Su, H. Liu, Y. Wang, Interconnected tin disulfide nanosheets grown on graphene for Li-ion storage and photocatalytic applications, ACS Appl. Mater. Interfaces, 5 (2013) 12073–12082.
[37] Y.C. Zhang, Z.N. Du, S.Y. Li, M. Zhang, Novel synthesis and high visible light photocatalytic activity of SnS_2 nanoflakes from $SnCl_2{\cdot}2H_2O$ and S powders, Appl. Catal. B, 95 (2010) 153–159.
[38] Y. Bai, X. Zong, H. Yu, Z.-G. Chen, L. Wang, Scalable low-cost SnS_2 nanosheets as counter electrode building blocks for dye-sensitized solar cells, Chem. Eur. J., 20 (2014) 8670–8676.
[39] Y. Sun, H. Cheng, S. Gao, Z. Sun, Q. Liu, Q. Liu, F. Lei, T. Yao, J. He, S. Wei, Y. Xie, Freestanding tin disulfide single-layers realizing efficient visible-light water splitting, Angew. Chem. Int. Ed., 35 (2012) 8727–8731.
[40] X. Yuan, H. Wang, Y. Wu, X. Chen, G. Zeng, L. Leng, C. Zhang, A novel SnS_2–$MgFe_2O_4$/reduced graphene oxide flower-like photocatalyst: solvothermal synthesis, characterization and improved visible-light photocatalytic activity, Catal. Commun., 61 (2015) 62–65.
[41] R. Lucena, F. Fresno, J.C. Conesa, Hydrothermally synthesized nanocrystalline tin disulphide as visible light-active photocatalyst: spectral response and stability, Appl. Catal. B, 415–416 (2012) 111–117.
[42] T. Yan, L. Li, G. Li, Y. Wang, W. Hu, X. Guan, Porous $SnIn_4S_8$ microspheres in a new polymorph that promotes dyes degradation under visible light irradiation, J. Hazard. Mater., 186 (2011) 272–279.
[43] S. Rengaraj, X.Z. Li, P.A. Tanner, Z. Pan, G.K.H. Pang, Photocatalytic degradation of methylparathion—an endocrine disruptor by Bi^{3+}-doped TiO_2, J. Mol. Catal. A: Chem., 247 (2006) 36–43.
[44] S. Rengaraj, S. Venkataraj, J.-W. Yeon, X.Z. Li, Y. Kim, G.K.H. Pang, Preparation, characterization and application of Nd–TiO_2 photocatalyst for the reduction of Cr(VI) under UV light illumination, Appl. Catal. B, 77 (2007) 157–165.
[45] Y.C. Zhang, Z.N. Du, K.W. Li, M. Zhang, Size-controlled hydrothermal synthesis of SnS_2 nanoparticles with high performance in visible light-driven photocatalytic degradation of aqueous methyl orange, Sep. Purif. Technol., 81 (2011) 101–107.
[46] A.R. Wang, H. Xiao, Controllable preparation of SnO_2 nanoplates and nanoparticles via hydrothermal oxidation of SnS_2 nanoplates, Mater. Lett., 63 (2009) 1221–1223.
[47] B.D. Cullity, J.W. Weymouth, Elements of X-ray diffraction, Am. J. Phys., 25 (1957) 394.
[48] P. Kubelka, F. Munk, Ein Beitrag zur Optik der Farban striche, Z. Tech. Phys., 12 (1931) 593–603.
[49] P. Kubelka, New contributions to the optics of intensely light-scattering materials, Part I, J. Opt. Soc. Am., 38 (1948) 448–457.
[50] R. López, R. Gómez, Band-gap energy estimation from diffuse reflectance measurements on sol–gel and commercial TiO_2: a comparative study, J. Sol-Gel Sci. Technol., 61 (2012) 1–7.
[51] R. Schlaf, P.G. Schroeder, M.W. Nelson, B.A. Parkinson, Observation of strong band bending in perylene tetracarboxylic dianhydride thin films grown on SnS_2, J. Appl. Phys., 86 (1999) 1499.
[52] C.D. Wagner, Handbook of X-ray Photoelectron Spectroscopy, Perkin–Elmer Corporation (1979).

[53] X. Chia, P. Lazar, Z. Sofer, J. Luxa, M. Pumera, Layered SnS versus SnS_2: valence and structural implications on electrochemistry and clean energy electrocatalysis, J. Phys. Chem. C, 120 (2016) 24098–24111.
[54] Y. Lei, S. Song, W. Fan, Y. Xing, H. Zhang, Facile synthesis and assemblies of flowerlike SnS_2 and In^{3+}-doped SnS_2: hierarchical structures and their enhanced photocatalytic property, J. Phys. Chem. C, 113 (2009) 1280–1285.
[55] Y.C. Zhang, L. Yao, G. Zhang, D.D. Dinoysiou, J. Li, X. Du, One-step hydrothermal synthesis of high-performance visible-light-driven SnS_2/SnO_2 nanoheterojunction photocatalyst for the reduction of aqueous Cr(VI), Appl. Catal. B, 144 (2014) 730–738.
[56] Y.C. Zhang, J. Li, M. Zhang, D.D. Dionysiou, Size-tunable hydrothermal synthesis of SnS_2 nanocrystals with high performance in visible light-driven photocatalytic reduction of aqueous Cr(VI), Environ. Sci. Technol., 45 (2011) 9324–9331.
[57] S. Park, J. Park, R. Selvaraj, Y. Kim, Facile microwave-assisted synthesis of SnS_2 nanoparticles for visible-light responsive photocatalyst, J. Ind. Eng. Chem., 31 (2015) 269–275.